The effect of reagent translation on the reaction dynamics and the absolute reaction cross section of H+H2O→OH+H2

ARTICLE *in* THE JOURNAL OF CHEMICAL PHYSICS · JANUARY 1994

Impact Factor: 2.95 · DOI: 10.1063/1.466546

3 AUTHORS, INCLUDING:

Axel Jacobs
Universität Heidelberg
17 PUBLICATIONS **515** CITATIONS

The effect of reagent translation on the reaction dynamics and the absolute reaction cross section of $H+H_2O \rightarrow OH+H_2$

A. Jacobs, H.-R. Volpp, and J. Wolfrum
Physikalisch Chemisches Institut der Universität Heidelberg, Im Neuenheimer Feld 253, 69120 Heidelberg, Germany

(Received 14 September 1993; accepted 13 October 1993)

With H atoms from ultraviolet laser photolysis of H_2S and HI, the influence of the translational excitation of the reagents on the reaction dynamics and the absolute value of the reaction cross section of $H+H_2O \rightarrow OH+H_2$ has been studied in the center of mass (c.m.) energy range from the reaction threshold up to 2.2 eV. To determine the OH product rotational fine-structure distributions, the nascent OH radicals were detected with quantum state resolution by laser-induced fluorescence (LIF). It was found that at all c.m. collision energies, the OH radicals are produced exclusively in the vibrational ground state. The measured $OH(v=0)$ rotational fine-structure distributions can be described by Boltzmann distributions, with rotational temperatures which increase only slightly with increasing collision energy. Near the threshold, the OH fine structure rotational temperatures are almost equal; at higher collision energies, the rotational temperature of the $OH(A')$ fine structure distribution is about a factor of 1.5 higher than the rotational temperature of the corresponding $OH(A'')$ fine-structure distribution, leading to preferential population of the symmetric $\Pi(A')$ state at high rotational quantum numbers. To investigate the influence of the reagents' translational energy on the reactivity, absolute reaction cross sections were measured at different collision energies. Using a calibration method to measure absolute number densities of nascent OH product radicals under single-collision conditions, the following absolute reaction cross sections were obtained: $\sigma_R(1.0\ \text{eV}) = (0.03 \pm 0.02)$ Å^2, $\sigma_R(1.5\ \text{eV}) = (0.16 \pm 0.05)$ Å^2, $\sigma_R(1.8\ \text{eV}) = (0.18 \pm 0.06)$ Å^2, $\sigma_R(2.2\ \text{eV}) = (0.25 \pm 0.07)$ Å^2. The experimental absolute reaction cross sections and OH rotational distributions are compared to the results of recent quasiclassical and quantum scattering calculations on an *ab initio* potential energy surface.

I. INTRODUCTION

The reaction

$$H+H_2O \rightarrow OH+H_2, \quad \Delta H_0^0 = 62\ \text{kJ/mol}, \qquad (1)$$

together with its reverse reaction (-1), has become a benchmark system for comparison between reaction dynamics theory of four-atom systems and quantum state-resolved experiments in recent years. Since the first pioneering quasiclassical trajectory (QCT) studies of Schatz *et al.*[1] in 1984, several other studies, quasiclassical[2] and quantum classical,[3] were carried out for reactions (1) and (-1). The first quantum scattering (QMS) calculations for reactions (1) and (-1) were reported by Clary[4] in 1991. In the meantime, further quantum calculations for reactions (1) and (-1) and its deuterated counterparts were reported by Bowman and Wang,[5] and Clary.[6] Recently, quantum mechanical calculations on the dynamics of reactions (1) and (-1) were also reported by Baer and co-workers,[7] where negative imaginary potentials were utilized to form absorbing boundary conditions.[8] In all of the quasiclassical and quantum calculations, the Walch–Dunning/Schatz–Elgersma (WD/SE) potential energy surface (PES) of the H–HOH(A') ground state,[9,10] or slightly modified versions of it, was used. The original WD/SE PES is characterized by a classical barrier of 0.923 eV for reaction (1), which is very close to the vibrational adiabatic barrier of 0.94 eV, reported in Ref. 11. Only recently were two new surfaces derived by Isaacson[12] which are able to reproduce both the *ab initio* information of Walch and Dunning[7] as well as the new barrier shape calculated by Dunning *et al.*[13]

On the experimental side, due to its great practical importance in hydrogen combustion, measurements of the thermal rate constant of reaction (-1) over an extended temperature range have been carried out.[14] The rate constant expression reported in Ref. 15, derived from direct measurements, shows non-Arrhenius behavior for reaction (-1) and is in good agreement with the corresponding expression calculated from the equilibrium constant and the measured rate constants of (1).[16] Experiments on the state-specific kinetic of reaction (-1) furthermore show that vibrational excitation in H_2 promotes reactivity more than vibrational excitation of OH.[17] Experimental results of the dynamics of $OH+D_2 \rightarrow HOD+D$ were reported in a recent communication by Casavecchia and co-workers,[18] who used the crossed molecular beams technique. Very recently, first reaction dynamics studies of reaction (-1) with translationally excited reactants were carried out.[19]

The first studies on the influence of translational excitation and isotopic substitution on the absolute reaction cross section of reaction (1) were reported by Wolfrum and co-workers.[20] Experiments on the dynamics of reaction (1) using translationally excited H atoms have also been reported by Kessler and Kleinermanns[21] and Honda *et al.*[22] In addition, the influence of vibrational excitation

 0021-9606/94/100(3)/1936/10/$6.00

of H_2O on the reaction dynamics of reaction (1) and is isotopically substituted counterparts has been studied in different experiments. The first example of mode-selective chemistry in the reaction of highly vibrationally excited H_2O/HOD with room temperature H atoms was reported by Crim and co-workers.[23] First experiments on the reaction of translationally excited H atoms with HOD/D_2O molecules, which are prepared only with low levels of vibrational excitation, were reported by Zare and coworkers.[24] In all of these experiments, OH/OD product radicals were detected. Only recently were HD product molecules from the reaction of translationally excited H atoms with D_2O molecules detected in Zare's group.[25] Also recently, first investigations were carried out by Lovejoy, Goldfarb, and Leone[26] on the rotational and vibrational excitation of water molecules by translationally excited H atoms.

All these experiments have contributed a lot to the understanding of the dynamics of reaction (1). However, as already mentioned in Ref. 18, due to the fact that the total (translational and/or vibrational) energy of the reactants in all these experiments is much higher than the reaction threshold, none of these experiments probed details of the minimum energy path on the potential energy surface. To get more detailed insight into the reaction dynamics of reaction (1) near the threshold, in the present study we used H atoms with a center of mass energy of 1.0 eV, an energy which is very close to the adiabatic reaction threshold of 0.94 eV.[11] A comparison of our measured OH rotational product state distributions at this collision energy with the results of QMS calculations of Nyman and Clary[27] and adiabatic-bend Franck–Condon (ABFC) calculations of Wang and Bowman[28] will be made.

To investigate the influence of the reagent translation on the reactivity and dynamics of reaction (1), we have furthermore measured absolute reactive cross sections and OH product rotational state distributions at different collision energies up to 2.2 eV. QMS calculations of absolute reaction cross sections and OH product state distributions, which have until now focused mainly on low collision energies, have recently been extended to higher collision energies typically used in "hot" H atom experiments. In Sec. IV, a detailed comparison of our results with the results of the recent QMS calculations by Nyman and Clary[27] mentioned above and recent quasiclassical trajectory (QCT) calculations by Kudla and Schatz,[29] as well as with results from previous experiments will be made.

II. EXPERIMENT

The experiments were carried out using the laser photolysis/laser induced fluorescence (LP/LIF) "pump–probe" technique. It is essentially the same method as that used to measure OH product quantum state distributions for reactions such as, e.g., $H+CO_2$ (Ref. 30) and $H+O_2$.[31] The experimental setup we used is depicted schematically in Fig. 1. The reaction was studied in a Teflon-coated quartz reactor equipped with long sidearms acting as a baffle system to keep scattered light out of the fluorescence collecting optics. The experiments were carried

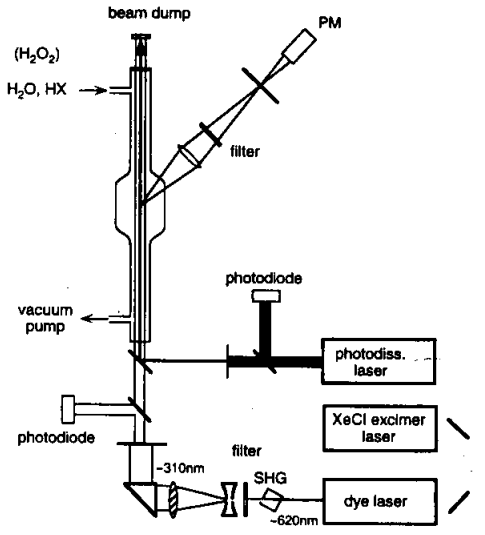

FIG. 1. A schematic diagram of the experimental setup.

out in flowing mixtures of HX [with HX being either H_2S Union Carbide (UCAR), electronic grade, or HI UCAR, 98%] and room temperature H_2O (double distilled) with a ratio of 1:10 at a total pressure of typically 55–70 mTorr (measured by a MKS Baratron). While H_2S was used without further purification, HI was pumped through a cooling trap to remove I_2 impurities before entering the reaction cell. For the calibration measurements, H_2O_2 was pumped through the cell at a total pressure of typically 10 mTorr. Prior to use, H_2O_2 (85% PEROXID Chemie) was pumped through the cell for at least three days until it reached a final concentration >99.8% (determined by titration). To prevent metal-surface-mediated decomposition of H_2O_2, an all-Teflon line was used to connect the H_2O_2 reservoir with the reaction cell. The gas flow into the cell was regulated with a glass valve. Special care was taken to ensure complete wall passivation of the reaction cell. Before each calibration measurement, H_2O_2 was pumped through the cell for at least 20 min until the cell pressure reached its final stability of >99%. Several test runs were performed to make sure that the flow rate in the reaction cell during the experiment was high enough to ensure total renewal of the gas in the sampled volume between two successive laser shots. By setting the probe pulse before the photodissociation pulse, we were not able to detect any OH signals from the preceding laser shot up to repetition rates of about 40 Hz.

Translationally excited H atoms were generated by photodissociation of the HX precursor using an excimer laser (Lambda LPX 205) with unstable resonator optics. The laser was operated with an ArF mixture (emission wavelength 193 nm) to photodissociate H_2S and with KrF mixture (emission wavelength 248 nm) to photodissociate H_2S and HI. In this case, both lasers (pump and probe) were operated at 20 Hz. A circular diaphragm with an aperture of 3 mm was used to skim off a homogeneously irradiated part of the unfocused rectangular excimer profile

to provide the photolysis beam. In addition, we used the fourth harmonic of a Nd:YAG laser (Spectra Physics GCR 11)to photodissociate HI at 266 nm. In this case, both lasers (pump and probe) were operated at 10 Hz. Typically, energies of 2 mJ/pulse at 193 nm (at this pulse energy, no OH background from the direct H_2O photolysis was detectable), 9 mJ/pulse at 248 nm and 5 mJ/pulse at 266 nm (measured with an energy detector Gentec ED 200) were used in the experiment. At these energies, we found that the OH signals from the reaction and the OH signals from the H_2O_2 photolysis show a linear dependence on the photolysis laser intensity, indicating the absence of two-photon processes in both the HX (see, e.g., Ref. 32) and H_2O_2 photodissociation. In addition, several test runs were carried out to determine the amount of OH radicals from the direct photodissociation of water. With the values for the photodissociation pulse energies mentioned above, we were not able to detect OH radicals when only water was present in the reactor. Therefore it was not necessary to apply the background correction procedure which has been used in our previous investigation,[20(b)] where HBr/H_2O mixtures were photolyzed at 193 nm.

Typically 60–150 ns after the photodissociation ("pump") pulse, the nascent OH product radicals were probed by a second copropagating ("probe") laser beam by laser induced fluorescence in the $A\,^2\Sigma^+ \leftarrow X\,^2\Pi$ system. The UV probe beam (bandwidth 0.2 cm^{-1}) in the wavelength region of 305–320 nm was provided by a frequency-doubled dye laser (Lambda FL 2002 EC) working with rhodamine B, pumped by a XeCl excimer laser (Lambda EMG 201 MSC). To ensure a linear dependence of the OH fluorescence on the probe laser intensity, the probe beam was attenuated and expanded with a telescope to a diameter of 12 mm and aligned to overlap the 3 mm diameter photolysis beam in the focus of observation. The emitted OH fluorescence was collected by a lens ($f=D=50$ mm) and projected through a 1×5 mm slit aperture and a UV filter (Schott UG 5, 1 mm) onto the cathode of a photomultiplier (EMI 9781 B, voltage 620 V). The LIF signal as well as the photolysis and probe intensities (both measured with photodiodes) were recorded with a three-channel boxcar system (SRS 250) and transferred to a microcomputer (HP series 9000, model 320, OS/HP-Basic) via an analog-to-digital converter (SRS 235). The OH fluorescence signal (recorded with a 100 ns boxcar gate, delayed by 10–20 ns from the probe pulse) was normalized to both laser intensities.

OH LIF spectra were recorded between 306.5 and 320 nm, where most of the $OH(A\,^2\Sigma^+,v'=0, 1\leftarrow X\,^2\Pi,v''=0,1)$ transitions are located. Line positions and identifications of the OH(A–X) transitions were taken from the fundamental work of Dieke and Crosswhite[33] and stored in a data file. By means of a computer program (written in HP-Basic), it was possible to divide the entire OH spectrum into "slow" and "fast" scanning regions. To save laser shots, in the fast scanning regions, where no OH transitions are located, the probe laser was scanned with a wavelength tuning step size ten times larger than the step size used in the slow scanning regions, where OH lines are expected.

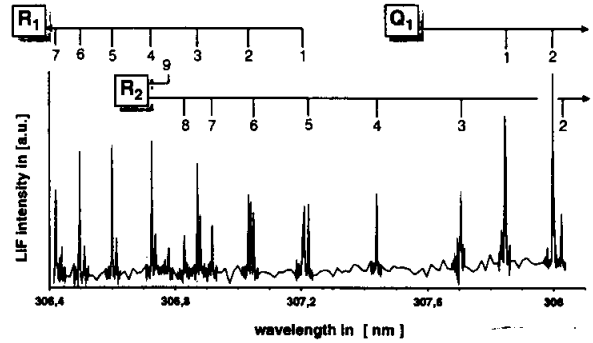

FIG. 2. Part of the $OH(A\,^2\Sigma^+,v'=0\leftarrow X\,^2\Pi,v''=0)$ LIF spectrum from the reaction $H+H_2O$ at $E_{c.m.}=1.8$ eV.

III. RESULTS

In Fig. 2 a typical OH LIF spectrum from reaction (1) is shown, which was recorded with the method described above. For clarity, only main branch lines are labeled. The hot H atoms were generated by 248 nm photolysis of HI. To obtain a satisfactory signal-to-noise (S/N) ratio, each point in this spectrum was averaged over 40 laser shots (in the case of 248 nm dissociation of H_2S, at least 80 laser shots had to be averaged to get a reasonable S/N ratio).

In our investigation, we spared no effort in searching for vibrationally excited OH radicals. For every collision energy used in our investigation (with the exception of the lowest collision energy, where the available energy is not high enough to populate OH vibrational states higher than $v=0$), several LIF spectra were recorded in the R_1 branch region of the $OH(A\,^2\Sigma^+,v'=1\leftarrow X\,^2\Pi,v''=1)$ band. In this wavelength region, also several P_1 lines of the $OH(A\,^2\Sigma^+,v'=0\leftarrow X\,^2\Pi,v''=0)$ band are located, which probe rotational levels that are reasonably well populated in the reaction. With experimental conditions described in the experimental part, which were chosen to ensure reagent single-collision conditions, no $OH(v=1)$ signals could be found besides the clearly detectable signals originating from the $OH(v=0)$ rotational levels. To enhance the sensitivity for $OH(v=1)$ detection, we used a method similar to that reported in Ref. 23(e). Therefore we have carried out several measurements at longer delay times and higher reactant pressures to allow about one gas kinetic collision of the nascent OH product radicals. Because the OH rotational relaxation is much faster than vibrational relaxation,[34] this should lead to higher population of the probed $OH(v=1, K=1,2,$ and $3)$ rotational levels (here and in the following parts of the article, the quantum number K, as defined in Hund's case (b),[35] is used to denote the OH rotational levels), as well as to an increase of the total amount of OH produced in the reaction. In addition, in these experiments, the probe laser intensity was increased until the $OH(v=0)$ P_1 transitions were clearly saturated. Under these conditions, we estimate the $OH(v=1)$ sensi-

tivity to be about ten times higher than under single-collision and unsaturated conditions. However, even with the abovementioned higher sensitivity, we could not detect any $OH(v=1)$ signals. We therefore determined from the present S/N ratio the upper limit for the $OH(v=1)/OH(v=0)$ ratio to be 0.01 for all collision energies. This rather small value suggests that there is unlikely to be significant population in the $OH(v=2)$ state, which would be rather difficult to detect [due to the predissociative character of the higher vibrational states in the electronically excited $OH(A\,^2\Sigma^+)$ state and the small off-diagonal transition probabilities with the LIF technique].

Relative number densities n_i of the $OH(v=0)$ radicals in the absorbing rotational level i were calculated using the following linear relationship:

$$I_{\text{meas},ik} = C n_i B_{ik} \nu_{ik} I_{\text{probe}} I_{\text{photo}} F(i,k), \tag{2}$$

where B_{ik} is the Einstein coefficient of absorption[36] and ν_{ik} is the wave number for the transition $i \rightarrow k$. I_{probe} is the probe laser intensity and I_{photo} is the intensity of the photodissociation laser. The factor C describes the effects of the detector system such as quantum efficiency, geometrical collection efficiency, etc. on the measured LIF intensity. $I_{\text{meas},ik}$ was determined by numerical integration of the corresponding spectral line profile $i \rightarrow k$ in the digitized LIF spectrum. Overlapping lines were deconvoluted by fitting separate Gaussian functions to the digitized LIF spectrum using a numerical least-squares fit procedure. For those branches where satellites and main lines overlap, the sum was determined and separated into components by the known ratio of the Einstein coefficients. $F(i,k)$ is a correction which had to be made because of the large rotational-level dependent quenching cross section of H_2O (Ref. 37) and H_2O_2 for $OH(A\,^2\Sigma^+)$.

A. OH rotational fine structure distributions

Due to the interaction between the spin of the unpaired electron and the electronic angular momentum, every rotational state in the electronic ground state of the OH radical is split into two spin–orbit states $\Pi_{1/2}$ and $\Pi_{3/2}$. In the rotating molecule, because of the interaction between the electronic angular momentum and the rotational angular momentum, every spin–orbit state splits further into two Λ components,[38] denoted as $\Pi(A')$ and $\Pi(A'')$ according to Ref. 39. In the high J limit [where Hund's case (b) description is appropriate], the $\Pi(A')$ Λ-doublet states can be characterized by the π molecular orbital being located in the plane of rotation, while in the case of the $\Pi(A'')$ Λ-doublet states, the π molecular orbital is oriented perpendicular to the plane of rotation. The electronic wave function of the $\Pi(A')$ Λ-doublet states is symmetric with respect to reflection of the spatial coordinates of the electrons in the plane of rotation, while the electronic wave function of the $\Pi(A'')$ Λ-doublet states is antisymmetric with respect to reflection. Because of the rigorous selection rules, R and P branch transitions can be used to probe the $\Pi(A')$ Λ-doublet states and Q branch transitions can be used to probe the $\Pi(A'')$ Λ-doublet states.

Figure 3 shows the rotational fine structure distribu-

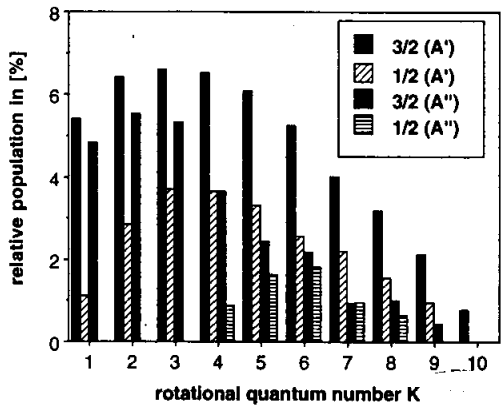

FIG. 3. Population distribution of the $OH(v=0)$ rotational fine structure states from reaction (1) at $E_{\text{c.m.}}=1.8$ eV.

tion of OH radicals produced in reaction (1), where the translationally excited H atoms ($E_{\text{c.m.}}=1.8$ eV) where generated by 248 nm photolysis of HI. From the relative population of the fine structure energy levels, we calculate the average OH rotational energy to be $\langle E_{\text{rot}} \rangle = 0.07$ eV. This means that only about 6% of the excess energy in the reaction appears in the OH rotational degree of freedom. At the other collision energies, we found similar behavior. At 1.0, 1.5, and 2.2 eV respectively, 12%, 8%, and 5% of the total available energy appears as rotational energy of the OH products.

In Ref. 22, it was found that at $E_{\text{c.m.}}=1.5$ eV, the relative population distribution of the symmetric $\Pi(A')$ and the antisymmetric $\Pi(A'')$ OH Λ-doublet components can be fit separately to Boltzmann distributions with markedly different rotational "temperatures" $T(A')$ and $T(A'')$. These temperatures should by no means be interpreted as being equal to the temperatures of canonical ensembles of products being in thermal equilibrium with a bath, because the nascent OH products actually belong to a nonequilibrium microcanonical ensemble. Nevertheless, these temperatures have the advantage of immediately giving a quantitative feeling for the relative population and the degree of rotational excitation. Therefore we also used this method even though from a more rigorous point of view the information theoretical approach developed by Levine, Bernstein, and co-workers[40] would be the more appropriate tool to characterize nascent product state distributions.

To study the dependence of the rotational excitation of the OH products on the collision energy, rotational temperatures were determined for each Λ-doublet component of the $OH(\Pi_{3/2})$ spin–orbit component (for which all rotational levels populated in the reaction can be probed by nonoverlapping R and Q line transitions) at different c.m. energies. In Table I the values of $T(A')$ and $T(A'')$ are listed and compared to the results of our previous work at $E_{\text{c.m.}}=2.5$ eV and to the results of other workers. From Table I, it can be seen that, in general, $T(A') > T(A'')$, with some dependence on the collision energy. This differ-

TABLE I. OH rotational temperatures of the $^2\Pi_{3/2}$ spin component at different c.m. energies. (a) from Ref. 22, (b) from Ref. 24(b), and (c) from Ref. 20(b).

$E_{c.m.}$ in [eV]	$T(A')$ in [K]	$T(A'')$ in [K]
1.0	550±90	510±80
	800±50[a]	550±30[a]
1.5	750±75[b]	
	810±70	530±60
1.8	850±65	520±70
2.2	870±40	550±60
2.5	920±60[c]	610±70[c]

[a]From Ref. 22.
[b]From Ref. 24(b).
[c]From Ref. 20(b).

ence in the rotational temperatures leads to a preference population of the $\Pi(A')$ states at high rotational quantum numbers. The population ratios $\Pi(A')/\Pi(A'')$ in the $\Pi_{3/2}$ manifold calculated from the measured fine-structure distributions are shown in Fig. 4 for the different collision energies used in the experiment. The Λ-doublet population ratio increases with increasing rotational quantum number as OH undergoes transition from Hund's coupling case (a) to Hund's coupling case (b). Similar behavior was found by Andresen and co-workers[41] for the inelastic scattering of $OH(^2\Pi_{3/2})$ with H_2.

On the other hand, we found that the ratio of the spin–oribt components $\Pi_{3/2}/\Pi_{1/2}$ [weighted by $K/(K+1)$ to account for the different degeneracies of the two spin–orbit states] is almost unity for all rotational states probed in the experiment. This reflects the fact that, in general, the rotational temperatures of the two spin–orbit components are almost equal $T(3/2) \approx T(1/2)$.

In Ref. 19, similar behavior was reported for the rotational fine structure distributions of OD radicals produced in the reaction $H+D_2O$.

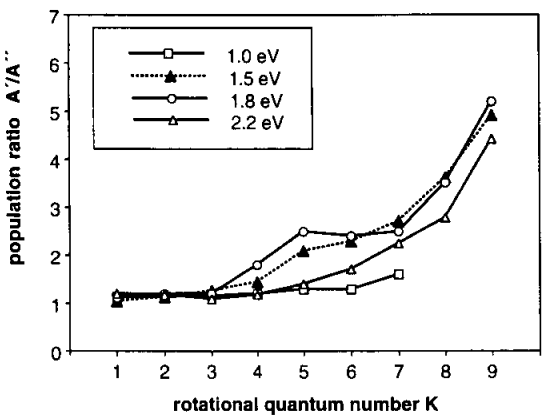

FIG. 4. Population ratio $\Pi(A')/\Pi(A'')$ of the $OH(v=0)$ Λ components at different collision energies.

B. Absolute reaction cross sections

Absolute reaction cross sections were measured using a method which was introduced by Kleinermanns and Wolfrum.[42] In this method, pulsed laser systems (with typical pulse durations of 8–10 ns) are used to measure absolute product number densities with a time resolution high enough to determine absolute reaction cross section under single collision conditions. The major goal of this method is the utilization of a well-defined OH radical source to calibrate unknown OH number densities obtained in the reaction.

For a single collision energy, the change of the total OH product number density from reaction (1) is given by

$$d[OH]^R(t)/dt = \sigma(v_{rel}) v_{rel} [H](t)[H_2O](t), \qquad (3)$$

where $[A](t)$ denotes the time-dependent concentration of species A. v_{rel} is the relative velocity of the reactants and $\sigma(v_{rel})$ is the corresponding absolute reaction cross section (which in the case of our measurements is always an average value over the room temperature rotational distribution of H_2O). For small t with only a small fraction of the initially generated H atoms reacted, $[H](t=0)=[H](t)=$const. and with $[H] \ll [H_2O]=$const.,

$$[OH]^R(t) = \sigma(v_{rel}) v_{rel} [H][H_2O] t \qquad (4)$$

is a solution of Eq. (3). With Eq. (4), it is possible to calculate absolute reaction cross sections from time-resolved OH absolute number density measurements. In our experiments, we used the photodissociation of H_2O_2 at 193, 248, and 266 nm as a source of well-defined absolute OH number densities. By comparison of relative OH number densities at the time t from the reaction [denoted as $n_{R,i}$, where i is an index which denotes the rotational fine structure state to be probed, calculated from the spectral lines using Eq. (2)] with relative OH number densities ($n_{C,i}$) from the H_2O_2 photodissociation, it is possible to relate the unknown OH number density $[OH]^R(t)$ from the reaction to the well-defined OH number density $[OH]^C(t)$ generated in H_2O_2 photodissociation, using the following expression:

$$[OH]^R(t)/[OH]^C(t) = (n_{R,i} f_{C,i})/(n_{C,i} f_{R,i}). \qquad (5)$$

Here $f_{R,i}$ and $f_{C,i}$ refer to the relative population of the fine structure state i which is probed in the reaction and the H_2O_2 photodissociation, respectively. t is the time interval between the photodissociation pulse (which defines the zero point of the reaction) and the subsequent probe laser pulse. Several test runs were carried out to verify that $[OH]^C(t)=[OH]^C(t=0)$ (which means that the OH number densities initially generated in the H_2O_2 photodissociation remain constant during the typical reaction time t), which will lead to a significant simplification in the expression we want to derive for the absolute reaction cross section. Therefore relative OH number densities (generated in the H_2O_2 photodissociation) were measured at different delay times t to determine the onset of OH flying out of the probe volume. In the 193 nm H_2O_2 photodissociation (which leads to the fastest OH radicals having a laboratory

velocity of about 4.6 km/s), we found that up to delay times of 250 ns, the relative OH number densities inside the probe volume remains constant within 2%.

The following linear relationships (which are valid if $I_{photo} \ll 1/\sigma^{HO}_{H_2O_2}$ and $I_{photo} \ll 1/\sigma^{HX}$):

$$[OH]^C(t=0) = I_{photo}\phi^{OH}\sigma^{H_2O_2}[H_2O_2], \quad (6)$$

$$[H](t=0) = I_{photo}\sigma^{HX}[HX] \quad (7)$$

were used to relate the initially generated OH, and H number densities to the HX and H_2O_2 number densities. Here I_{photo} denotes the photolysis laser photon flux, and $\sigma^{H_2O_2}$ and σ^{HX} denote the absorption cross sections of H_2O_2 and the H atom precursors, respectively. ϕ^{OH} is the corresponding OH quantum yield in the H_2O_2 photodissociation at the corresponding wavelength. Inserting Eqs. (5) and (6) into Eq. (4), the following expression can be derived:

$$\sigma = (I_{R,i} f_{C,i} \phi^{OH}\sigma^{H_2O_2}[H_2O_2])/(I_{C,i} f_{R,i}\sigma^{HX}[HX] \times [H_2O] t v_{rel}), \quad (8)$$

which now consists of directly measurable parameters. The number densities $[H_2O_2]$, [HX], and $[H_2O]$ were calculated from the corresponding partial pressures. Values for the H_2O_2 absorption cross sections $\sigma^{H_2O_2}$ and the corresponding quantum yields ϕ^{OH} were taken from Ref. 43. Absorption cross sections for HI at 248 and 266 nm were taken from Ref. 44 and multiplied with the $I(^2P_{3/2})/I(^2P_{1/2})$ branching ratios[44] to account for the fact that at both photodissociation wavelengths, only the fast H atoms which belong to the $H+I(^2P_{3/2})$ dissociation channel have enough energy to overcome the reaction barrier. Absorption cross sections for H_2S at 248 and 193 nm were taken from Ref. 45. The 248 nm absorption cross section of H_2S was multiplied by 0.945 [the $SH(v=0)$ quantum yield] to account for the fact that only H atoms which belong to this dissociation channel have enough translational energy to react. The relative reagent velocity v_{rel} was calculated from energy and momentum conservation of the HX photodissociation at the given photolysis wavelength of the experiment using the formulas given in Ref. 46. Values for the HX dissociation energies were taken from Ref. 44. In the case of H_2S photodissociation at 193 nm, the average relative reagent velocity was calculated from the average laboratory velocity, which was determined by weighted averaging over the measured H atom velocity distribution reported in Ref. 47. The delay time t was determined directly by measuring the time difference between the pump and probe stray light pulses on a fast oscilloscope (Tektronix model 485, 350 MHz).

As one can see from Eq. (8) prior to the measurement of the absolute reaction cross section, the complete OH vibrational and rotational distributions for the reaction and the H_2O_2 photolysis had to be determined. After this, a single spectral OH line starting from one fine structure level i was recorded in the reaction. After flushing the cell with N_2 (for at least 30 min), H_2O_2 was flowed through the reactor (again for at least 20 min, to ensure complete wall passivation of the reaction cell) and the same OH spectral line was recorded in the H_2O_2 photodissociation. With this procedure, which was repeated several times for different nonoverlapping Q, P, and R branch spectral lines, we determined the following absolute reactive cross sections for reaction (1):

$$\sigma_R(1.0\ eV) = (0.03 \pm 0.02)\ Å^2,$$

$$\sigma_R(1.5\ eV) = (0.16 \pm 0.05)\ Å^2,$$

$$\sigma_R(1.8\ eV) = (0.18 \pm 0.06)\ Å^2,$$

$$\sigma_R(2.2\ eV) = (0.25 \pm 0.07)\ Å^2.$$

Each of the following values represents the mean value calculated from at least six independent calibration measurements using the method described above. The experimental error was calculated from the errors of the entries of Eq. (8) on the basis of simple error propagation. Errors of the absorption cross sections and quantum yields were taken from the corresponding references.

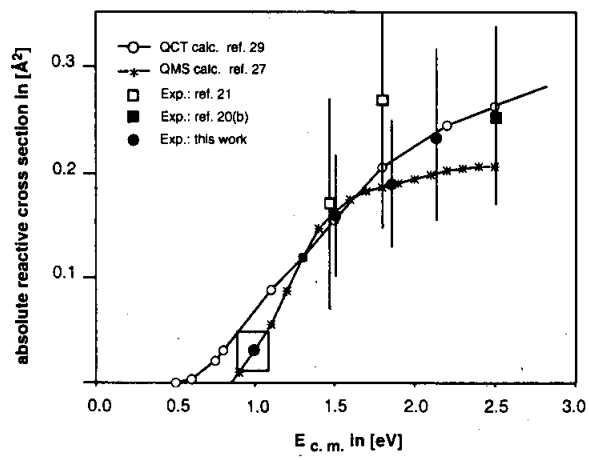

FIG. 5. Absolute reactive cross section of the reaction $H+H_2O \rightarrow OH+H_2$.

IV. DISCUSSION

A. Absolute reactive cross sections

In Fig. 5, our experimental values are compared to the results of recent quasiclassical trajectory (QCT)[29] and most recent QMS calculations[27] on the WD/SE PES. The QMS calculations were performed using the rotating bond approximation (RBA),[4] which has been found, by comparison with very recent exact planar four-atom quantum calculations,[48] to give accurate reaction probabilities for reactions (1) and (−1). Both the QCT and the QMS calculations were carried out for nonrotating H_2O in the vibrational ground state (0,0,0). In previous QCT studies,[1(a)] it was found that averaging of $H_2O(0,0,0)$ initial rotational angular momentum states typically populated at room temperature is not important for calculating absolute reaction cross sections for reaction (1). The same behavior was found in the abovementioned exact planar

four-atom quantum calculations[48] so the theoretical values depicted in Fig. 8 are appropriate for comparison with experiments using room temperature H_2O.

The width of the box in Fig. 5, which was drawn around the experimental absolute reaction cross sections at $E_{c.m.}=1.0$ eV, represents the full width at half-maximum (FWHM) of the underlying experimental collision energy distribution schematically. It was calculated using the formulas reported in Ref. 49 and includes the spread which comes from the thermal motion of the H_2S precursor and the H_2O reactant, as well as the spread due to the SH rotational excitation of the $SH(v=0)$ fragment in the 248 nm photodissociation of H_2S.[44]

As can be seen in Fig. 5, the QCT and QMS absolute reaction cross sections are in almost good agreement with our present experimental results as well as with the results of previous experiments. The fact that the QCT cross sections are clearly larger than the experimental and the QMS cross sections at low collision energies is due probably to the deficiency of classical mechanics in conserving zero point energy of the reactants.

B. OH vibrational and rotational excitation

The absence of vibrational excitation of the OH product radicals from reaction (1) shows clearly that the reaction (where H_2O is in the vibrational ground state) proceeds adiabatically with respect to the nonreacting bond. This is in good agreement with previous experimental observations[20(a),20(b),21,22,24(b)] and with the results of recent quantum mechanical studies,[7(a)] as well as with earlier QCT studies[1(a)] of reaction (1). In a generalized transition-state picture, the abovementioned spectator behavior of the nonreacting OH bond can be attributed to the *dynamics*, controlled by the relatively small transition-state region of the PES. A comparison of the OH bond length of the nonreacting OH bond at the transition state[50] with the equilibrium values in the H_2O and OH molecules shows that the OH bond length is almost unchanged in going from reagents through the transition state to the products.

On the other hand, the OH product rotational state distribution is characterized by the *kinematics* of the reaction and is therefore largely controlled by the masses of the particles and the transition-state geometry. In Ref. 51, the H–H–O–H transition state was found to be bent and planar, with the H–O–H angle being very close to that in the free H_2O molecule, with an O–H–H angle of 15°. Different models have been developed to explain the generally small OH rotational excitation in reaction (1). In Ref. 20(a), an impulsive model has been discussed, in which the recoil of the H_2 product molecule from the O atom through the bent transition-state configuration produces a torque which leads to OH product rotation. In this model, the degree of OH rotational excitation is limited by the small mass of the H_2 fragment and the small "lever arm," defined by the distance between the center of mass of the OH molecule and the O atom.

A simple stripping model was discussed in Refs. 1(a) and 20(c), where the OH rotational excitation is produced by simply mapping reagent (H_2O) bend excitation onto

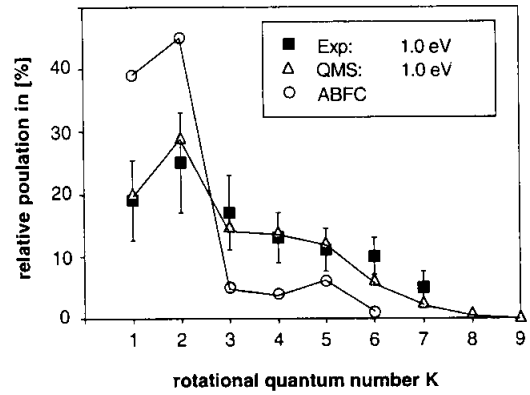

FIG. 6. A comparison of the measured rotational distribution and the theoretical QMS distribution from Ref. 27 at $E_{c.m.}=1.0$ eV. Results from the adiabatic-bend Franck–Condon (ABFC) calculations (Ref. 28) for the H–H–O–H ground bending state are also included.

the OH rotation. Following the earlier work of Schatz and Ross[52] on atom–diatom reactions, Wang and Bowman[28] developed a four-atom adiabatic-bend Franck–Condon (ABFC) model to calculate OH and H_2 rotational state distributions for reaction (1). The results of their calculations showed that HHOH bending excitation up to five quanta leads to generally "cold" OH rotational distributions. Since the ABFC calculation in the present form does not contain any dynamic information explicitly (i.e., in these calculations the OH product rotational distributions do not depend on the initial collision energy), a direct comparison with the experimental distributions at higher collision energies is not possible. However, a qualitative comparison of the experimental OH rotational distributions with the ABFC OH distributions (especially with those of the ground and first excited HHOH bend states) suggests that even at the highest collision energies used in the experiments, only a small number of energetically low-lying HHOH bend states are populated in the reaction. In Fig. 6, the experimental OH rotational distribution at $E_{c.m.}$

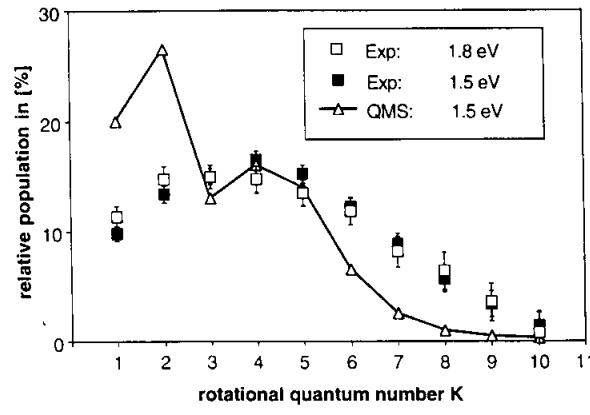

FIG. 7. A comparison of the experimental rotational distributions at $E_{c.m.}=1.5$ and 1.8 eV with the QMS results for $E_{c.m.}=1.5$ eV from Ref. 27.

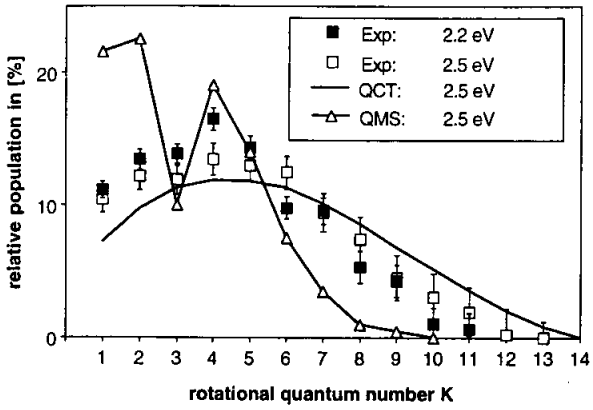

FIG. 8. A comparison of the experimental rotational distributions at $E_{c.m.}=2.2$ and 2.5 eV with the QMS results from Ref. 27 and the QCT results from Ref. 1(a), both for $E_{c.m.}=2.5$ eV.

$=1.0$ eV is compared to the ABFC ground bend state OH rotational distribution. At this energy (which is very close to the reaction threshold energy), the ground bend state would be expected to be the dominant bend state. Indeed, the reasonable agreement between the two distributions suggests that in the threshold region, OH product rotation is, at least to a large extent, dominated simply by the ground bending motion of the HHOH transition state.

In addition, the results of QMS calculations by Nyman and Clary[27] for $E_{c.m.}=1.0$ eV are included in Fig. 6. As one can see, the agreement between the QMS distribution (calculated invoking the RBA and centrifugal sudden approximation) and the experimental one is almost perfect. In Fig. 7, the experimental OH rotational distributions for $E_{c.m.}=1.8$ and 1.5 eV are depicted and compared to the QMS distribution calculated for $E_{c.m.}=1.5$ eV. In Fig. 8, experimental OH rotational distributions obtained at $E_{c.m.}=2.2$ and 2.5 eV [Ref. 20(b)] are compared to the QMS and to the QCT distribution[1(a)] calculated for $E_{c.m.}=2.5$ eV. At this point, it should be noted that the QMS calculations at all collision energies have been performed for $\Omega=0$, where Ω is the projection quantum number of J (the total angular momentum) and j (the rotational quantum number of OH) along $\mathbf{R}_1$ (the vector connecting the OH center of mass with the H_2 center of mass).

From the experimental distributions (which now cover the wide range between 1.0 and 2.5 eV), it can be seen that OH product rotation is rather insensitive to collision energy. Even the energy dependence found in the QMS calculations is somewhat smaller; the overall agreement between the QMS and the experimental OH rotational distribution is reasonable. In Ref. 27, the deviation of the QMS OH distributions from the experimental ones at higher energies was attributed to the fact that in the RBA used in the calculations, the H_2 rotation is not treated explicitly. Possibly, QMS RBA calculations for $\Omega>0$ could also give OH rotational distributions which may lead to better agreement between the theoretical and experimental distributions at higher collision energies. On the other hand, as one can see in Fig. 8, at high energies, the QCT method leads to a OH rotational distribution[1(a)] which is in very good agreement (apart from a small shift to slightly higher rotational quantum numbers, which may originate from the fact that zero-point energy of the reactants is not conserved in the quasiclassical treatment) with the experimental distribution.

C. Selective population of the Λ-doublet states of OH

Different methods—classical,[53] quasiclassical,[31(b)] and quantum mechanical[54]—have been applied to predict preference population of either A' or A'' Λ-doublet states of OH radicals produced in photodissociation and bimolecular reactive scattering processes as well as in inelastic collisions involving OH radicals.

In Ref. 53(a), a simple geometrical model was developed which predicts a $\Pi(A')/\Pi(A'')$ ratio of two for Π state molecules AB produced in the reaction $A+BC \rightarrow ABC^{\ddagger} \rightarrow AB+C$ if there is no preferred dissociation geometry of the transition state $ABC^{\ddagger}$. A somewhat different treatment was presented in Ref. 53(b), where the Λ-doublet formation of OH radicals produced in reactions of the type $H+OX \rightarrow OH+X$ was examined in detail. In this article, it was demonstrated that a dynamical anisotropy of the reactive cross section could lead to any value for the $\Pi(A')/\Pi(A'')$ ratio between 0 and ∞. Both treatments,[53] however, are only applicable to reactions where the OH bond is newly formed during the reactive collision.

Mainly classical models have been discussed to explain qualitatively the markedly different rotational temperatures of the OH Λ-doublet components and the generally larger cross section for $OH(A')$ formation in reaction (1). The higher rotational temperature of the $OH(A')$ Λ-doublet component was attributed to the fact that for a bent and planar HHOH transition state, product repulsion is channeled predominantly into in-plane rotation of the OH products with the unpaired orbital of the broken bond left in the plane of rotation.

If one considers the transition state region of a bimolecular reaction to be similar to the Franck–Condon region in the photodissociation process, following the general principles outlined by Schinke,[55] originally developed to explain the selective Λ-doublet state population in the photodissociation of water,[56] the preferential population of the $OH(A')$ Λ-doublet component at high J in reaction (1) simply reflects symmetry conservation of the electronic wave function of the reactive transition state ($^2A'$ in C_S geometry[9]). As one can see in Fig. 4, this picture can obviously give also only a qualitatively correct description, because in the high J limit it would predict, in contrast to the experimental results, the population to be exclusively in the $OH(A')$ Λ-doublet state. Besides the abovementioned strict correlation rule, transitions between adiabatic PESs can occur as a result of the breakdown of the Born–Oppenheimer approximation.

The multi-PES character of reaction (1) arises from the fact that the electronic symmetry which is well defined in the reactants $H_2O(^1A')$ and $H(^2A')$ actually breaks down in the OH product radical due to the interaction

between the electronic angular momentum and the nuclear rotation. This makes a complete conservation of symmetry in reaction (1) impossible. A combination of the symmetries of the $OH(X\,^2\Pi)$ and $H_2(X\,^1\Sigma_g^+)$ products for coplanar geometries leads to two adiabatic PESs $V_{A'}$ of $^2A'$ and $V_{A''}$ of $^2A''$ symmetry, respectively, for which only the $V_{A'}$ PES correlates with the reactants H_2O ($^1A'$) and $H(^2A')$.[9] As already mentioned in the Introduction, all theoretical reaction dynamics studies of reaction (1) were carried out on an *ab initio* representation of the $V_{A'}$ PES, but in none of these studies was the $^2\Pi$ character of the OH radical treated explicitly. On the other hand, quantum mechanical methods[54] invoking both $V_{A'}$ and $V_{A''}$ PESs have been applied successfully to reproduce the preference population of the $\Pi(A')$ Λ-doublet state in inelastic collisions of $OH(^2\Pi_{3/2})$ with H_2. In Ref. 54, it was shown that for this reaction, the scattering dynamics is governed by the average $V^+ = V_{A''} + V_{A'}$ and the difference $V^- = V_{A''} - V_{A'}$ PESs rather than by the individual adiabatic PESs. The preferential population of Λ-doublet states was found to arise from the interference of the scattering amplitudes from V^+ and V^-. Similarities between the OH Λ-doublet state populations were found for $OH+CO$ and $OH+N_2$ low energy inelastic collisions[57] and the corresponding hot H atom reactions $H+CO_2$ [Ref. 30(d) and 30(f)] and $H+N_2O$ (Ref. 58), respectively. As discussed in detail in Ref. 59, product fine-structure features in reactive scattering can originate from effects in the transition-state region as well as from exit channel coupling effects. Therefore, similarity in the fine-structure distributions for reactive and inelastic processes is expected for those reactions where the subsequent inelastic scattering in the exit channel is the dominant effect. A comparison of our present results and the results from previous experiments by Honda *et al.*,[22] Wolfrum and collaborators,[20(a),20(b)] and Zare and co-workers[24(c)] with the Λ-doublet state distribution measured in the $OH(^2\Pi_{3/2})+H_2$ inelastic scattering experiments by Andresen and co-workers[41] suggests clearly that reaction (1) fits into this category.

V. CONCLUSIONS

Absolute reaction cross sections and OH rotational fine structure state distributions were measured for the reaction $H+H_2O$ at different collision energies.

The absolute reaction cross sections and the total OH rotational distributions (averaged over the fine-structure states) at the highest collision energies are in very good agreement with results of QCT calculations on the $HHOH(^2A')$ ground state $V_{A'}$ PES. At these collision energies, the QMS calculations on a slightly modified version of the same PES lead to lower reaction cross sections and "colder" OH rotational distributions. At lower collision energies, the QMS reaction cross sections are in excellent agreement with the experimental ones. The same holds for the OH rotational distributions at the lowest collision energy (1.0 eV) used in the experiments. On the other hand, the QCT calculations lead to markedly higher reaction cross sections at collision energies near the reaction threshold, where zero-point effects are expected to play a major role. As a matter of fact, modification of the theoretical treatment in order to account for zero-point effects in the quasiclassical, as well as to include higher Ω values in the QMS (RBA) calculations, would be a worthwhile goal and could probably lead to even better agreement between theoretical and experimental absolute reaction cross sections and total OH rotational distributions over the whole range of collision energies.

The measured OH fine-structure state distributions, at higher collision energies show a marked preference population for the symmetric OH $\Pi(A')$ states with a Λ-doublet ratio $\Pi(A')/\Pi(A'')$ of the $OH(^2\Pi_{3/2})$ spin–orbit component similar to that found in the inelastic collision of $OH(^2\Pi_{3/2})$ with H_2. Our results are consistent with a qualitative picture in which the transition state region of the $V_{A'}$ ground state PES dominates reactivity as well as product energy partitioning, while subsequent transitions between the two adiabatic PESs $V_{A'}$ and $V_{A''}$ in the OH–H_2 product exit channel are responsible for the nonstatistical population of the final OH Λ-doublet components. However, for a detailed quantitative comparison between theory and experiment, extension of the present theoretical methods in order to account for the multiple PES character of reaction (1) is clearly necessary.

ACKNOWLEDGMENTS

The financial support of the Deutsche Forschungsgemeinschaft is gratefully acknowledged. The authors wish to thank M. Baer, J. M. Bowman, P. Casavechia, D. C. Clary, G. C. Schatz, and R. N. Zare for sending preprints of their publications and I. Bar and S. Rosenwaks for helpful communications. Thanks are also due to G. Nyman for very stimulating discussions.

[1] (a) G. C. Schatz, J. L. Colton, and M. C. Grant, J. Phys. Chem. **88**, 2971 (1984); (b) H. Elgersma and G. C. Schatz, Int. J. Quantum. Chem. Symp. **15**, 611 (1981); (c) G. C. Schatz, J. Chem. Phys. **74**, 1133 (1981); (d) G. C. Schatz and S. P. Walch, *ibid.* **72**, 776 (1980).
[2] N. J. Brown and O. Rashed, J. Chem. Phys. **82**, 5506 (1985); **85**, 4348 (1986); J. A. Harrison and H. R. Mayne, *ibid.* **87**, 3698 (1987); **88**, 7424 (1988); K. Kudla and G. C. Schatz, Chem. Phys. Lett. **193**, 507 (1992); J. Chem. Phys. **95**, 8267 (1991).
[3] G. D. Billing, Chem. Phys. **146**, 63 (1990).
[4] D. C. Clary, J. Chem. Phys. **95**, 7298 (1991).
[5] (a) D. Wang and J. M. Bowman, J. Chem. Phys. **96**, 8906 (1992); (b) J. M. Bowman and D. Wang, *ibid.* **96**, 7852 (1992); (c) D. Wang and J. M. Bowman, *ibid.* (preprint).
[6] (a) D. C. Clary, J. Chem. Phys. **96**, 3656 (1992); (b) Chem. Phys. Lett. **192**, 34 (1992).
[7] (a) H. Szichman, I. Last, A. Baram, and M. Baer, J. Phys. Chem. **97**, 6436 (1993); (b) H. Szichman, I. Last, and M. Baer, J. Phys. Chem. (to be published).
[8] (a) D. Neuhauser and M. Baer, J. Phys. Chem. **94**, 185 (1990); (b) M. Baer and D.Neuhauser, J. Chem. Soc., Faraday Trans. **86**, 1721 (1990); (c) M. S. Child, Mol. Phys. **72**, 89 (1991); (d) I. Last, D. Neuhauser, and M. Baer, J. Chem. Phys. **96**, 2017 (1992); (e) T. Seideman and W. H. Miller, *ibid.* **96**, 4412 (1992).
[9] S. P. Walch and T. H. Dunning, J. Chem. Phys. **72**, 1303 (1980).
[10] G. C. Schatz and H. Elgersma, Chem. Phys. Lett. **73**, 21 (1980).
[11] D. G. Truhlar and A. D. Issacson, J. Chem. Phys. **77**, 3516 (1982).
[12] A. D. Isaacson, J. Phys. Chem. **96**, 531 (1992).
[13] T. H. Dunning, L. B. Harding, and E. Kraka, in *Supercomputer Algorithms for Reactivity, Dynamics, and Kinetics of Small Molecules*, edited by A. Laganà (Kluwer, Dordrecht, The Netherlands, 1989), pp. 57–71.
[14] P. Frank and Th. Just, Ber Bunsenges. Phys. Chem. **89**, 198 (1985); A.

R. Ravishankara, J. M. Nicovich, R. L. Thompson, and F. P. Tully, J. Phys. Chem. **85**, 2498 (1981); F. P. Tully and A. R. Ravishankara, *ibid.* **80**, 3126 (1980).
[15] R. C. Oldenborg, G. W. Loge, D. M. Harradine, and K. R. Winn, J. Phys. Chem. **96**, 8425 (1992).
[16] (a) J. V. Michael and J. W. Sutherland, J. Phys. Chem. **92**, 3853 (1988); (b) D. F. Davidson, A. Y. Chang, and R. K. Hanson, *International 22nd Symposium on Combustion* (The Combustion Institute, Pittsburgh, 1988), p. 1877.
[17] (a) J. E. Spencer, H. Endo, and G. P. Glass, *16th International Symposium on Combustion* (The Combustion Institute, Pittsburgh, 1976), p. 829; (b) G. C. Light and J. H. Matsumo, Chem. Phys. Lett. **58**, 578 (1978); (c) R. Zellner and W. Steinert, *ibid.* **81**, 568 (1981).
[18] M. Alagia, N. Balucani, P. Casavecchia, D. Stranges, and G. G. Volpi, J. Chem. Phys. **98**, 2459 (1993).
[19] S. Koppe, T. Laurent, P. D. Naik, H.-R. Volpp, and J. Wolfrum, Can. J. Chem. (to be published).
[20] (a) K. Kleinermanns and J. Wolfrum, Appl. Phys. B **34**, 5 (1984); (b) A. Jacobs, H.-R. Volpp and J. Wolfrum, *24th International Symposium on Combustion* (The Combustion Institute, Pittsburgh, 1992), p. 605; (c) A. Jacobs, H.-R. Volpp, and J. Wolfrum, Chem. Phys. Lett. **196**, 249 (1992).
[21] K. Kessler and K. Kleinermanns, Chem. Phys. Lett. **190**, 145 (1992).
[22] K. Honda, M. Takayanagi, T. Nishiya, H. Ohoyama, and I. Hanazaki, Chem. Phys. Lett. **180**, 321 (1991).
[23] (a) A. Sinha, M. C. Hsiao, and F. F. Crim, J. Chem. Phys. **92**, 6333 (1990); (b) A. Sinha, J. Phys. Chem. **94**, 4391 (1990); (c) F. F. Crim, M. C. Hsiao, J. L. Scott, A. Sinha, and R. L. van der Wal, Philos. Trans. R. Soc. London Ser. A **332**, 259 (1990); (d) A. Sinha, M. C. Hsiao, and F. F. Crim, J. Chem. Phys. **94**, 4928 (1991); (e) M. C. Hsiao, A. Sinha, and F. F. Crim, J. Phys. Chem. **95**, 8263 (1991); (f) F. F. Crim, A. Sinha, M. C. Hsiao, and J. D. Thoemke, in *Mode Selective Chemistry*, edited by J. Jortner, R. D. Levine, B. Pullman (Kluwer, Dordrecht, The Netherlands, 1991), p. 217.
[24] (a) M. J. Bronikowski, W. R. Simpson, B. Girad, and R. N. Zare, J. Chem. Phys. **95**, 8647 (1991); (b) M. J. Bronikowski, W. R. Simpson, and R. N. Zare, J. Phys. Chem. **97**, 2194 (1993); (c) **97**, 2204 (1993).
[25] D. E. Adelman, S. V. Filset, and R. N. Zare, J. Chem. Phys. **98**, 4636 (1993).
[26] C. M. Lovejoy, L. Goldfarb, and S. R. Leone, J. Chem. Phys. **96**, 7180 (1992).
[27] G. Nyman and D. C. Clary, J. Chem. Phys. (to be published).
[28] D. Wang and J. M. Bowman, Chem. Phys. Lett. **207**, 227 (1993).
[29] K. Kudla and G. C. Schatz, J. Chem. Phys. **98**, 4645 (1993).
[30] (a) C. R. Quick and J. J. Tie, Chem. Phys. Lett. **100**, 223 (1983); (b) K. Kleinermanns and J. Wolfrum, *ibid.* **104**, 157 (1984); (c) K. Kleinermanns, E. Linnebach, and J. Wolfrum, J. Phys. Chem. **89**, 2525 (1985); (d) G. Radhakrishnan, S. Buelow, and C. Wittig, J. Chem. Phys. **84**, 727 (1986); (e) J. Rice, G. Hoffmann, and C. Wittig, *ibid.* **88**, 2841 (1988); (f) A. Jacobs, M. Wahl, R. Weller, and J. Wolfrum, Chem. Phys. Lett. **158**, 161 (1989); (g) G. Hoffmann, D. Oh, Y. Chen, Y. M. Engel, and C. Wittig, Isr. J. Chem. **30**, 115 (1990); (h) N. F. Scherer, C. Sipes, R. B. Bernstein, and A. H. Zewail, J. Chem. Phys. **92**, 5239 (1990).
[31] (a) K. Kleinermanns and J. Wolfrum, J. Chem. Phys. **80**, 181 (1984); (b) K. Kleinermanns, E. Linnebach, and M. Pohl, *ibid.* **91**, 2181 (1989); (c) M. J. Bronikowski, R. Zhang, D. J. Rakestraw, and R. N. Zare, Chem. Phys. Lett. **156**, 7 (1989); (d) A. Jacobs, H.-R. Volpp, and J. Wolfrum, Ber. Bunsenges. Phys. Chem. **94**, 1390 (1990); (e) A. Jacobs, H.-R. Volpp, and J. Wolfrum, Chem. Phys. Lett. **177**, 200 (1991); (f) K. Kessler and K. Kleinermanns, J. Chem. Phys. **97**, 374 (1992).
[32] R. E. Continetti, B. A. Balko, and Y. T. Lee, Chem. Phys. Lett. **182**, 400 (1991).
[33] G. H. Dieke and H. M. Crosswhite, J. Quant. Spectrosc. Radiat. Transfer **2**, 97 (1962).
[34] K. H. Gerike and F. J. Comes, J. Chem. Phys. **65**, 113 (1982); G. A. Raiche, J. B. Jeffries, K. J. Rensberger, and D. R. Crosley, *ibid.* **92**, 7258 (1990).
[35] G. Herzberg, *Molecular Spectra and Molecular Structure* (Van Nostrand, Princeton, 1950), Vol. 1.
[36] I. L. Chidsey and D. R. Crosley, J. Quant. Spectrosc. Radiat. Transfer **23**, 187 (1980).
[37] R. A. Copeland, M. J. Dyer, and D. R. Crosley, J. Chem. Phys. **82**, 4022 (1985).
[38] R. N. Zare, *Angular Momentum* (Wiley, New York, 1988).
[39] M. H. Alexander, P. Andresen, R. Bacis, R. Berson, F. J. Comes, P. J. Dagdigijan, R. N. Dixon, R. W. Field, G. W. Flynn, K.-H. Gericke, E. R. Grant, B. J. Howard, J. R. Huber, D. S. King, J. L. Kinsey, K. Kleinermanns, K. Kuchitsu, A. C. Luntz, A. J. McCaffery, B. Pouilly, H. Reisler, S. Rosenwaks, E. W. Rothe, M. Shapiro, J. P. Simons, R. Vasedev, J. R. Wiesenfeld, C. Wittig, and R. N. Zare, J. Chem. Phys. **89**, 1749 (1988).
[40] R. B. Bernstein and R. D. Levine, J. Chem. Phys. **57**, 434 (1972); A. Ben-Shaul, R. D. Levine, and R. B. Bernstein, *ibid.* **57**, 5427 (1972); Chem. Phys. Lett. **15**, 160 (1973); R. D. Levine and R. B. Bernstein, Acc. Chem. Res. **7**, 393 (1974); R. D. Levine and J. L. Kinsey, in *Atom–Molecule Collision Theory—A Guide for the Experimentalist*, edited by R. B. Bernstein (Plenum, New York, 1979), p. 693.
[41] P. Andresen, D. Häusler, and H. W. Lülf, J. Chem. Phys. **81**, 571 (1984); P. Andresen, N. Aristov, V. Beushausen, D. Häusler, and H. W. Lülf, *ibid.* **95**, 5763 (1991).
[42] K. Kleinermanns and J. Wolfrum, Chem. Phys. **80**, 1446 (1984).
[43] G. L. Vaghjiani and A. R. Ravishankara, J. Chem. Phys. **92**, 996 (1990); G. L. Vaghjiani, A. A. Turnipseed, R. F. Warren, and A. R. Ravishankara, *ibid.* **96**, 5878 (1992).
[44] G. N. A. van Veen, K. A. Mohamed, T. Baller, and A. E. de Vries, Chem. Phys. **74**, 261 (1983).
[45] C. A. Wight and S. R. Leone, J. Chem. Phys. **78**, 4875 (1983); **79**, 4823 (1983).
[46] W. J. van der Zande, R. Zhang, R. N. Zare, K. G. McKendrick, and J. J. Valentini, J. Phys. Chem. **95**, 8205 (1991).
[47] R. E. Contineti, B. A. Balko, and Y. Lee, Chem. Phys. Lett. **182**, 400 (1991).
[48] J. Echave and D. C. Clary, J. Chem. Phys. (to be published).
[49] (a) G. N. A. van Veen, K. A. Mohamed, T. Baller, and A. E. de Vries, Chem. Phys. **74**, 261 (1983); (b) S. Koppe, T. Laurent, P. D. Naik, H.-R. Volpp, J. Wolfrum, T. Arusi-Parpar, I. Bar, and S. Rosenwaks, Chem. Phys. Lett. (in press).
[50] G. C. Schatz and H. Elgersma, Chem. Phys. Lett. **73**, 21 (1980).
[51] G. C. Schatz and H. Elgersma, in *Potential Energy Surfaces and Dynamics Calculations*, edited by D. Truhlar (Plenum, New York, 1981).
[52] G. C. Schatz and J. Ross, J. Chem. Phys. **66**, 1037 (1977).
[53] (a) M. Bronikowski and R. N. Zare, Chem. Phys. Lett. **166**, 5 (1990); (b) I. Hanazaki, *ibid.* **201**, 301 (1993).
[54] (a) R. Schinke and P. Andresen, J. Chem. Phys. **81**, 5644 (1984); (b) P. J. Dagdigian, M. H. Alexander, and K. Liu, *ibid.* **91**, 839 (1989); (c) D. P. Dewangan, D. R. Flower, and G. Danby, J. Phys. B **19**, L 747 (1986).
[55] R. Schinke, *Photodissociation Dynamics* (Cambridge University, Cambridge, 1993).
[56] P. Andresen, G. S. Ondrey, B. Titze, and E. W. Rothe, J. Chem. Phys. **80**, 2548 (1984).
[57] D. M. Sonnefroh, R. G. Macdonald, and K. Liu, J. Chem. Phys. **94**, 6508 (1991).
[58] W. E. Hollingsworth, J. Subbiah, G. W. Flynn, and R. E. Weston, Jr., J. Chem. Phys. **82**, 2295 (1985); H. Ohoyama, M. Takayanagi, T. Nishiya, and I. Hanazaki, Chem. Phys. Lett. **162**, 1 (1989).
[59] R. G. Macdonald and K. Liu, J. Chem. Phys. **93**, 2431 (1990); **93**, 2443 (1990).